

Shape Optimization of Energy Dissipation Devices for Passive Seismic Control of Building Frames

Hidekazu Watanabe¹, Makoto Ohsaki¹ and Junki Nozoe¹

¹Department of Architecture, Hiroshima University, Kagamiyama 1-4-1, Higashi-Hiroshima, 739-8527, Japan; PH: +81-82-424-7800; email: {hidekazu-watanabe, ohsaki, m124850}@hiroshima-u.ac.jp

ABSTRACT

Optimization results are presented for improving energy dissipation capacity of passive seismic control devices under cyclic deformation. The locations and thicknesses of the stiffeners, as well as the aspect ratio, of a shear-type hysteretic steel damper are optimized to improve energy dissipation capacity under static cyclic deformation. A general-purpose finite element software package is used for elastoplastic analysis, and a heuristic optimization algorithm called tabu search is utilized for optimization after discretization of variables into integer values. The objective function is the dissipated energy before the maximum value of equivalent plastic strains among all elements reaches the upper bound under the prescribed loading condition, and constraints on reaction force and moment are incorporated by penalty function approach. The material parameters of the low-yield-point steel are identified through optimization also using tabu search.

INTRODUCTION

Hysteretic steel dampers such as shear panels are widely used for passive seismic control of building frames in seismic-prone regions. The input energy of seismic excitation is dissipated through plastic deformation under cyclic motion. The geometrical and material parameters of such dampers are usually determined from experimental results and simplified analysis based on frame models. However, the physical experiments demand substantial cost, and the accuracy of the simple analysis mode is not enough for predicting behavior of the device and frame under seismic motion. Therefore, it is desired to design the devices through optimization with prediction of responses using a high-precision finite element analysis. The second author demonstrated through a series of studies that the performances of structural parts including beams and braces can be successfully improved through heuristic optimization algorithms combined with high-precision finite element analysis (Pan et al. 2007, Ohsaki and Nakajima 2012).

The authors optimized the geometrical parameters of a shear panel damper, which is located between the upper and lower beams of a story, and consists of a

low-yield-point steel panel that dissipates seismic energy under forced interstory deformation (Watanabe et al. 2012). The shear panel is stiffened by several stiffeners to prevent local buckling that leads to premature fracture before a sufficient amount of energy is dissipated. However, in Watanabe et al. (2012), the material parameters are assigned empirically, and the height of the panel is optimized by enumeration of parameters discretized into integer values.

In this study, we optimize the locations and thicknesses of the stiffeners as well as the aspect ratio of the shear panel using a heuristic optimization method called tabu search (Glover 1989) (hereafter referred to as TS). The elastoplastic responses under static cyclic loading are evaluated using a general-purpose finite element analysis software package called ABAQUS (Dassault Systems 2011). The parameters of constitutive relation of the low-yield-point steel, defined using a nonlinear isotropic-kinematic hardening model, are also identified through optimization using TS.

OPTIMIZATION PROBLEM AND OPTIMIZATION ALGORITHM

We use TS, which is classified as a single-point local search (Ohsaki 2010), and has been developed for optimization problem with integer variables. TS basically moves to the best neighborhood solution even if it does not improve the current solution. A tabu list is used to prevent an unfavorable phenomenon called cycling, in which several solutions are selected alternatively.

Real variables X_1, \dots, X_m are defined by integer variables J_1, \dots, J_m with the specified standard value X_{i0} and increment ΔX_i as

$$X_i = X_{i0} + J_i \Delta X_i \quad (i = 1, \dots, m) \quad (1)$$

Therefore, all of the objective and constraint functions are defined by the vector of integer variables $\mathbf{J} = (J_1, \dots, J_m)$, where J_m is selected from s_i integer values. We consider an optimization problem for maximizing the objective function $F(\mathbf{J})$. The constraints are given as $g_j(\mathbf{J}) \leq g_{j0}$ ($j = 1, \dots, n$), where g_{j0} is the specified upper bound. The optimization problem is formulated as follows:

$$\text{Maximize} \quad F(\mathbf{J}) = E_p(\mathbf{J}) \quad (2a)$$

$$\text{subject to} \quad g_j(\mathbf{J}) \leq g_{j0} \quad (j = 1, \dots, n) \quad (2b)$$

$$J_i \in \{1, 2, \dots, s_i\}, \quad (i = 1, \dots, m) \quad (2c)$$

In order to apply TS, the constraints are incorporated into the objective function through penalty function approach, as demonstrated in the numerical examples.

The basic algorithm of TS for a maximization problem is summarized as follows:

Step 1 Randomly generate a seed solution $\mathbf{J} = (J_1, \dots, J_m)$ and initialize the tabu list T as $T = \{\mathbf{J}\}$. Evaluate the objective function and initialize the incumbent

optimal objective value as $F_{\text{opt}} = F(\mathbf{J})$.

- Step 2** Generate a set of q neighborhood solutions $\mathbf{J}^{\text{Nj}} = (J_1^{\text{Nj}}, \dots, J_m^{\text{Nj}})$, ($j = 1, \dots, q$) from \mathbf{J} , and evaluate the objective function of each solution.
- Step 3** Among the solutions in the set $\{\mathbf{J}^{\text{N1}}, \dots, \mathbf{J}^{\text{Nq}}\}$, select the best one that has the maximum value of objective function, and is not included in the list T . Assign the best solution as the new seed solution \mathbf{J} .
- Step 4** Update the incumbent optimal objective function as $F_{\text{opt}} = F(\mathbf{J})$ when the value is improved.
- Step 5** Add the seed solution \mathbf{J} to the list T if the size of tabu list is less than the prescribed limit.
- Step 6** Output F_{opt} and the corresponding optimal solution, if the number of iterations reaches the specified value; otherwise, go to Step 2.

In Step 2, the neighborhood solution $\mathbf{J}^{\text{Nj}} = (J_1^{\text{Nj}}, \dots, J_m^{\text{Nj}})$ is defined as follows using uniform random numbers r :

$$r < 0.3333: \quad J_i^{\text{Nj}} = J_i - 1 \quad (3a)$$

$$0.3333 \leq r < 0.6667: \quad J_i^{\text{Nj}} = J_i \quad (3b)$$

$$r \geq 0.6667: \quad J_i^{\text{Nj}} = J_i + 1 \quad (3c)$$

Fig. 1 shows the data flow between TS and FE-analysis using ABAQUS Ver.6.11 (Dassault Systems 2011). The pre-process and post-process are carried out using the python script. The computations of functions and the process of TS are coded using FORTRAN.

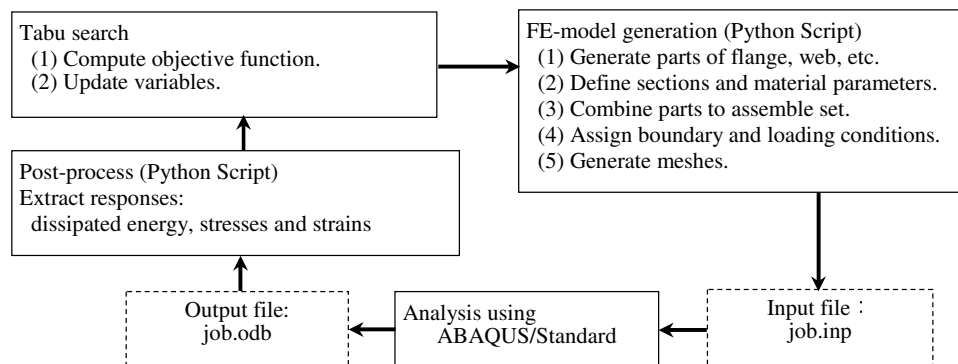


Figure 1. Optimization algorithm using TS and ABAQUS.

SHEAR-TYPE HYSTERETIC STEEL DAMPER

Shear-panel damper model. The material parameters are identified and the analysis results are verified using the experimental results of the shear-type hysteretic steel damper as shown in Fig. 2 (Izumi *et al.* 1996). The size of the specimen is 2/3 of the real size. The specimen is a stud-type viscoelastic damper, which is extensively used

as passive control device of seismic responses of building frames. The material of center shear panel of the device, indicated as hatched area in Fig. 2, is a low-yield-point steel. When the device is attached between the beams, the panel yields due to the interstory shear force prior to the bracket of the device and other members of a frame. This way, the panel zone can dissipate the earthquake energy efficiently without damaging other parts. The buckling restraining stiffeners are assigned to prevent premature out-of-plane buckling of the panel. The stiffeners are located longitudinally in the front side, and laterally in the rear side of the panel.

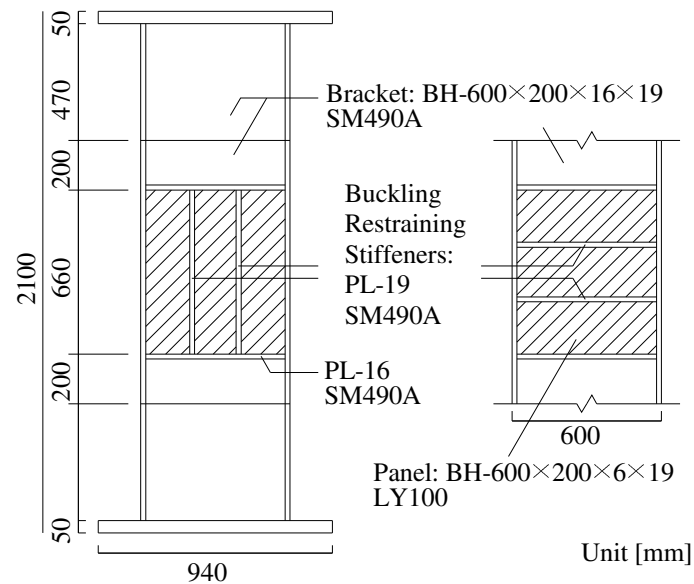


Figure 2. Experimental specimen; left: front side, right: rear side).

The material of the panel, flanges, and buckling restraining stiffeners are LY100 (low-yield-point steel), SM490A, and SS400, respectively. The values of Young's modulus E , Poisson's ratio ν , yield stress σ_y , and tensile strength σ_u obtained by uniaxial tests are listed in Table 1.

Table 1. Material properties.

	E [N/mm ²]	ν	σ_y [N/mm ²]	σ_u [N/mm ²]
LY100	200000	0.3	98	254
SM490A (PL-19)	200000	0.3	345	537
SM490A (PL-16)	200000	0.3	367	545
SS400	200000	0.3	368	442

Constitutive Model. A finite element model of the experimental specimen in Fig. 2 is generated using python script. A quadrilateral thick shell element called S4R is used, and the nominal size of mesh is 40 mm for automatic mesh generation. A linear kinematic hardening rule is used for SM490A and SS400, where the hardening ratio is

0.001 E . In contrast, a nonlinear isotropic-kinematic hardening rule, defined as follows, is used for LY100 (low-yield-point steel).

Using stress tensor σ_{ij} and initial yield stress σ_y , the initial yield function $F(\sigma_{ij})$ and subsequent yield function $F(\sigma_{ij}, \alpha_{ij}, \bar{\varepsilon}^{pl})$ are defined as

$$F(\sigma_{ij}) = \varphi(\sigma_{ij}) - \sigma_y^2 = 0 \quad (4a)$$

$$f(\sigma_{ij}, \alpha_{ij}, \bar{\varepsilon}^{pl}) = \varphi(\sigma_{ij} - \alpha_{ij}) - [\sigma_0(\bar{\varepsilon}^{pl})]^2 = 0 \quad (4b)$$

where α_{ij} , $\bar{\varepsilon}^{pl}$ and $\sigma_0(\bar{\varepsilon}^{pl})$ are backstress tensor, equivalent plastic strain and the radius of subsequent yield function, respectively. $\varphi(\sigma_{ij} - \alpha_{ij})$ denotes equivalent stress, which is defined as

$$\varphi(\sigma_{ij} - \alpha_{ij}) = \frac{3}{2}(s_{ij} - \bar{\alpha}_{ij})(s_{ij} - \bar{\alpha}_{ij}) \quad (5)$$

where s_{ij} is deviator stress tensor, $\bar{\alpha}_{ij}$ is deviatoric component of backstress tensor. Nonlinear kinematic hardening part is defined as the sum of the Ziegler kinematic hardening rule and relaxation term for the nonlinearity as

$$\dot{\alpha}_{ij}^k = C \frac{1}{\sigma_0} (\sigma_{ij} - \alpha_{ij}) \dot{\bar{\varepsilon}}^{pl} - \gamma \alpha_{ij}^k \dot{\bar{\varepsilon}}^{pl} \quad (6a)$$

$$\alpha_{ij} = \sum_{k=1}^N \alpha_{ij}^k \quad (6b)$$

where C and γ are initial hardening ratio and reduction ratio of kinematic hardening, respectively, which are material parameters identified from the structural experiment. N is the number of function for the backstress. In the isotropic hardening part, the radius of subsequent yield function $\sigma_0(\bar{\varepsilon}^{pl})$ is defined as follows:

$$\sigma_0(\bar{\varepsilon}^{pl}) = \sigma_y + Q_\infty(1 - e^{-b\bar{\varepsilon}^{pl}}) \quad (7)$$

where Q_∞ and b are material parameters identified by the structural experiment. Q_∞ is the maximum increase of radius of yield function; b is the increase ratio of yield function depending on equivalent plastic strain.

Parameter Identification. The material parameters γ , Q_∞ , and b are identified through optimization for minimizing the difference between the responses by analysis and experiment. The initial hardening ratio C is defined as 0.001 E for simplicity. It is possible to utilize a material test for parameter identification; however, cyclic material test is very difficult to carry out. Furthermore, our purpose is to accurately predict the cyclic response of the panel attached to the frame. Therefore, the results of the test in

Fig. 1 are used for parameter identification.

A vertical forced displacement equivalent to a compressive axial force of 710 kN is applied at the top plate prior to the forced horizontal cyclic deformation. The loading program of the static shear force of 2.25 cycles is controlled by the forced displacement as shown in Fig. 3.

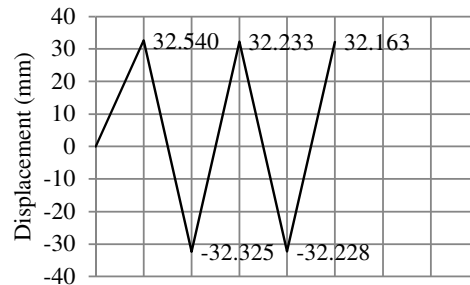


Figure 3. Forced displacement for parameter identification.

The objective function to be minimized is the norm τ_{rms} of difference between the shear stresses τ_i^{exp} by experiment and τ_i^{ana} by analysis, which is defined as

$$\tau_{rms} = \sqrt{\frac{1}{M} \sum_{i=1}^M (\tau_i^{exp} - \tau_i^{ana})^2} \quad (8)$$

where M is the number of data in the experiment. The available data of experiment are shown in Fig. 4(a). Since the data are not uniformly distributed, and the accuracy in plastic loading range is more important than that in elastic or unloading range, the data for identification are selected as shown in Fig.4(b).

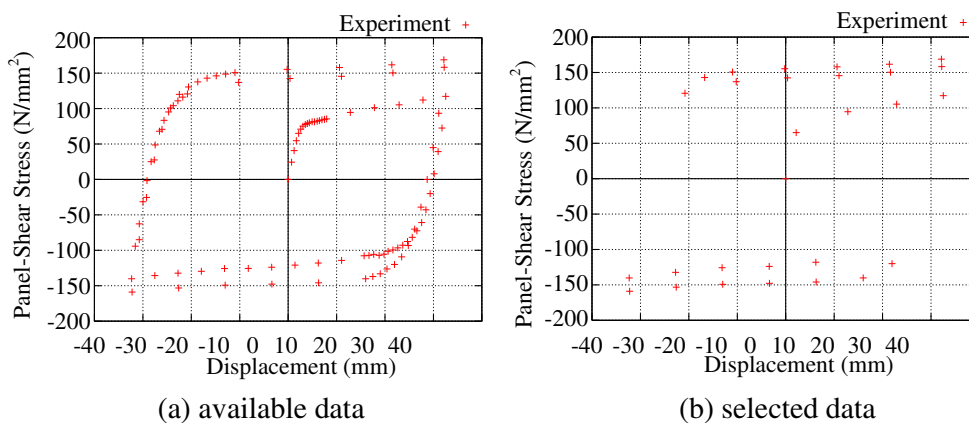


Figure 4. Experimental results of displacement-stress relation.

In the optimization problem for parameter identification, the vector of variables consists of the material parameters: γ , Q_∞ , and b , which are defined in terms of integer variables J_1 , J_2 , and J_3 as

$$\gamma = 600 + J_1 \times \Delta\gamma \quad J_1 \in \{1, 2, \dots, 7\} \quad (9a)$$

$$Q_\infty = \sigma_y + J_2 \times \Delta Q_\infty \quad J_2 \in \{1, 2, \dots, 7\} \quad (9b)$$

$$b = 10 + J_3 \times \Delta b \quad J_3 \in \{1, 2, \dots, 7\} \quad (9c)$$

where $\Delta\gamma$, ΔQ_∞ , and Δb are 200, $0.1\sigma_y$, and 2, respectively. For the TS, the number of neighborhood solutions is $q = 3$, and the number of steps $n = 15$. The best parameter values obtained from three trials of TS from random initial solutions are listed in Table 2. The hysteresis loops of the experiment and the optimal parameter values are shown in Fig.5.

Table 2. Best parameter values obtained from optimization by TS.

C [N/mm ²]	γ [N/mm ²]	Q_∞ [N/mm ²]	b
200	2000	$1.4\sigma_y$	16

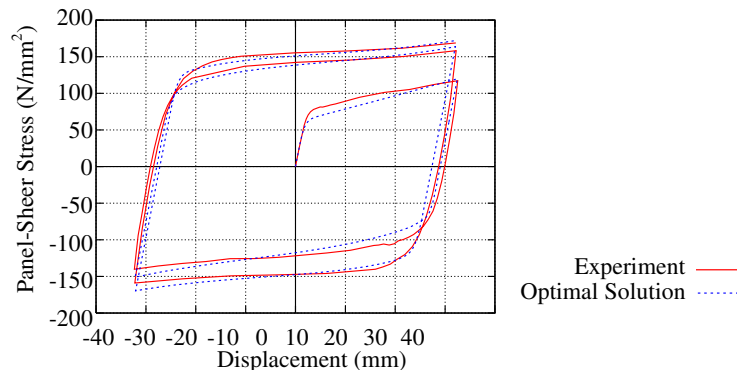


Figure 5. Hysteresis loop of the panel using best parameter values.

Standard Model. A finite element model called the Standard model is generated using the material parameters in Table 2. The constant displacement is applied at the top plate prior to the forced horizontal cyclic deformation in the same manner as the previous section. The loading program of the static shear force of five cycles is controlled by the peak drift angle of $1/60$ rad. There have been many criteria proposed for ductile fracture of steel materials. However, we use the equivalent plastic strain as a measure of damage of the material, because most of the criteria are based on the equivalent plastic strain.

The results of Standard model are shown in Table 3, where E_p , ϵ_{\max} , R_{\max} , and M_{\max} denote the total dissipated energy, the maximum equivalent plastic strain among all elements, the maximum horizontal reaction force, and the maximum reaction moment, respectively. Fig. 6 shows distribution of equivalent plastic strain of the standard model at final step. It can be observed from this figure that the equivalent plastic strain has larger values mainly in the red region around the center of the shear

panel.

The results of another model called Standard model-F are also shown in Table 3. The nominal size of mesh in the model is reduced to 30 mm from 40 mm. It is seen from Table 3 that difference of each response quantity is not large. Thus, considering the computation time, the Standard model with 40 mm mesh is used in optimization.

Table 3. Analysis results of standard model.

Model name	E_p [kN·m]	ε_{\max}	R_{\max} [kN]	M_{\max} [kN·m]
Standard model	256.0	0.802	591.0	585.0
Standard model-F	261.5	0.907	581.3	575.8

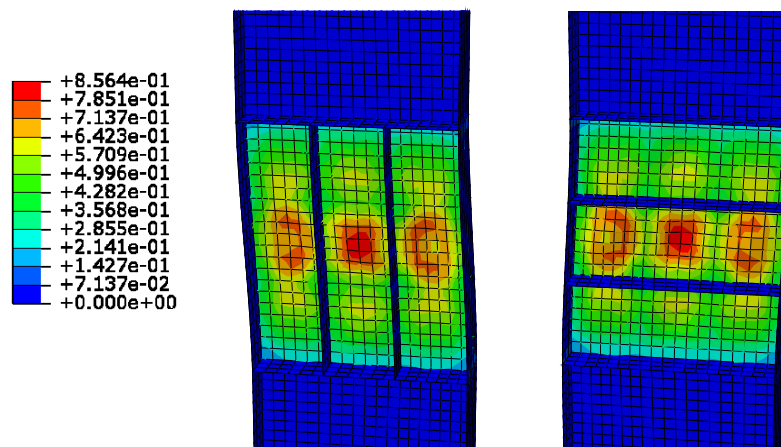


Figure 6. Distribution of equivalent plastic strain of the standard model at final step; left: front side, right: rear side.

OPTIMIZATION OF SHEAR-TYPE HYSTERETIC STEEL DAMPER

In this section, we demonstrate in the numerical examples that the performance of a shear-type hysteretic steel damper can be successfully improved by optimization. First, the locations and thicknesses of the buckling restraining stiffeners are optimized. Second, aspect ratio of the panel and variables in the first problems are optimized simultaneously. The objective function to be maximized is the total dissipated energy E_p when the maximum value of equivalent plastic strain among all elements reaches ε_{\max} of the standard model.

Optimization of locations and thicknesses of buckling restraining stiffeners. In this optimization problem, the vector of design variables consists of the locations of the buckling restraining stiffeners (K_1, K_2) and the thicknesses of the stiffeners (S_1, S_2). In order to preserve the symmetry, the numbers of independent variables for location and thickness are one, respectively, for the stiffeners in front and rear. The location X_i of the stiffeners at each side is defined by K_1 and K_2 as

$$X_i = K_i \times \Delta X_i \quad K_i \in \{1, 2, \dots, 7\} \quad (i = 1, 2) \quad (10)$$

where ΔX_1 and ΔX_2 are 1/18 of the width and height of the panel, respectively. The independent variables for thicknesses T_1 and T_2 of the stiffeners in two sided are defined by S_1 and S_2 as

$$T_i = 0.002 + S_i \times \Delta T_i \quad S_i \in \{1, 2, \dots, 8\} \quad (i = 1, 2) \quad (11)$$

where ΔT_1 and ΔT_2 are 0.001 m.

For the TS, the number of neighborhood solutions is $q = 4$, and the number of steps $n = 15$. Optimization is carried out from two different random initial solutions to investigate dependence of the optimal solution on the initial solution. The solution with larger value 301.0 [kN·m] for E_p is regarded as the optimal solution. The optimal values of this solution are $(K_1, K_2, S_1, S_2) = (3, 1, 8, 8)$. The optimal model and its 30mm-mesh-size model are hereafter called the opt-S and the opt-S-F, respectively. As the result of optimization, the total dissipated energy E_p is improved by 25.0 % from the standard model-F. The number of cycles before reaching the specified bound of maximum strain is 6.1. The distribution of equivalent plastic strain of the opt-S-F at final step is shown in Fig. 7.

Table 4. Analysis results of opt-S.

Model name	E_p [kN·m]	ε_{\max}	R_{\max} [kN]	M_{\max} [kN·m]
Standard model	256.0	0.802	591.0	585.0
opt-S	301.0	0.802	606.6	601.9
Standard model-F	261.5	0.907	581.3	575.8
opt-S-F	326.9	0.907	599.8	595.6

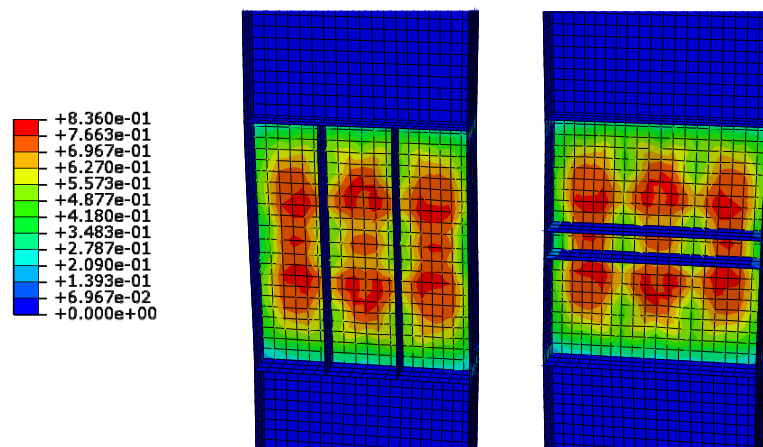


Figure 7. Distribution of equivalent plastic strain of opt-S-F at final step; left: front side, right: rear side.

In this optimal solution, the lateral buckling restraining stiffeners in the rear side are shifted to the center and the thicknesses of stiffeners in both sides are increased from the Standard model. It is seen from Figs. 6 and 7 that the equivalent plastic strain has large value in wider region as a result of optimization so that the large deformation

around the center of the standard model is restrained by moving the lateral stiffeners in the rear side to the center. This way, the energy dissipation property can be improved through this optimization.

In this model, the effect of optimization is summarized as follows:

1. More energy can be dissipated by increasing the area of large plastic deformation.
2. The maximum equivalent plastic strain can be reduced by increasing the stiffnesses of the stiffeners; hence, the number of cycles before reaching the specified bound of maximum strain can be increased.

Optimization of locations and thicknesses of stiffeners and aspect ratio of the panel. In this section, we optimize the thicknesses and locations of the buckling restraining stiffeners, as well as the aspect ratio of the panel, simultaneously. In order to preserve symmetry property, the independent variables of the aspect ratio of the panel are the panel width H_1 and the panel height H_2 , which are defined by two integer variables R_1 and R_2 as

$$H_1 = (R_1 + 7) \times \Delta H_1 \quad L_1 \in \{1, 2, \dots, 5\} \quad (12)$$

$$H_2 = (R_2 + 7) \times \Delta H_2 \quad L_2 \in \{1, 2, \dots, 8\} \quad (13)$$

where ΔH_1 and ΔH_2 are 1/10 of the width and height, respectively, of the panel of the Standard model. The vectors of design variables are K , S and L defined in Equations (10)-(13).

Although larger horizontal reaction R_{\max} leads to larger energy dissipation, larger R_{\max} and the maximum reaction moment M_{\max} may also lead to damage in frame members attached to the damper. Thus, upper bounds should be assigned for R_{\max} and M_{\max} in the process of optimizing the aspect ratio. In the following, the values of standard model are chosen as the upper bounds R_{\max}^0 and M_{\max}^0 .

Since TS cannot be used directly for a constrained optimization problem, the optimization problem with constraints is converted to unconstrained problem using the penalty function approach. The objective function $F(\mathbf{J})$ is replaced by the extended objective function $F'(\mathbf{J})$ using constraint functions $g_1(\mathbf{J})$ and $g_2(\mathbf{J})$ as follows:

$$F'(\mathbf{J}) = F(\mathbf{J}) \left\{ 1 - p \sum_{i=1}^2 \max \left(1 - \frac{1}{(g_i(\mathbf{J}))^2}, 0 \right) \right\} \quad (14a)$$

$$g_1(\mathbf{J}) = \frac{R_{\max}(\mathbf{J})}{R_{\max}^0} \leq 1 \quad (14b)$$

$$g_2(\mathbf{J}) = \frac{M_{\max}(\mathbf{J})}{M_{\max}^0} \leq 1 \quad (14c)$$

where penalty parameter p is equal to 0.25.

For the TS, the number of neighborhood solutions is $q = 6$, and the number of

steps $n = 15$. Optimization is carried out from three different random initial solutions to investigate dependence of the optimal solution on the initial solution. The number of analyses for obtaining an approximate optimal solution is about 90, which is very small compared with the total number of combination 125440 ($= 7 \times 7 \times 8 \times 8 \times 5 \times 8$).

The solution with largest value 392.5 [kN·m] for E_p is regarded as the optimal solution. The optimal values of this solution are $(K_1, K_2, S_1, S_2, L_1, L_2) = (3, 1, 5, 6, 3, 8)$. The optimal model and its 30mm-mesh-size model are hereafter called the opt-SW and the opt-SW-F, respectively. The opt-SW-F achieves 67.8% increase of the total dissipated energy E_p from the standard model. The number of cycles before reaching the specified bound of maximum strain is 8.4. The distribution of equivalent plastic strain of opt-SW-F at final step is shown in Fig. 8.

Table 5. Analysis results of opt-SW.

Model name	E_p [kN·m]	ϵ_{\max}	R_{\max} [kN]	M_{\max} [kN·m]
Standard model	256.0	0.802	591.0	585.0
opt-SW	392.5	0.801	548.5	549.7
Standard model-F	261.5	0.907	581.3	575.8
opt-SW-F	438.9	0.907	544.8	545.9

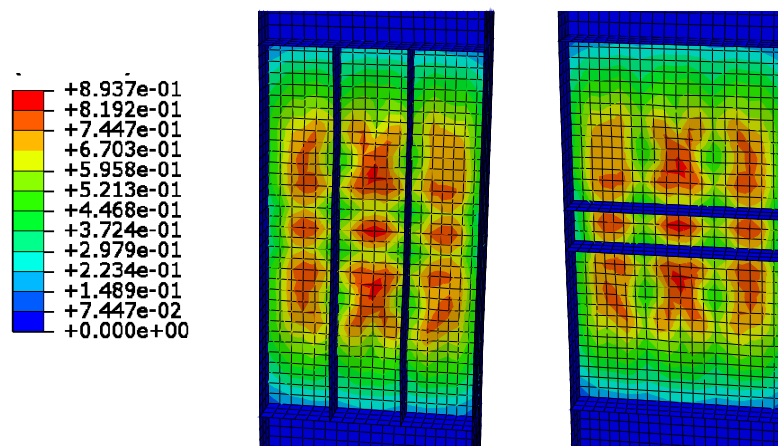


Figure 8. Distribution of equivalent plastic strain of opt-SW-F at final step; left: front side, right: rear side.

CONCLUSIONS

Optimization has been carried out for a shear-type hysteretic steel damper subjected to static cyclic deformation. The objective function is the total dissipated before the maximum equivalent stress reaches the specified value. The conclusions drawn from this study are summarized as follows:

1. A heuristic approach called TS can be effectively used to obtain an approximate of a computationally expensive structural optimization problem with practically

- acceptable small number of function evaluations.
2. The material parameters of nonlinear isotropic-kinematic hardening can also be identified using the TS for minimizing the error between the experimental and analysis results.
 3. The optimization algorithm using the TS and the penalty function approach has been proposed for a constrained problem. Using this method, energy dissipation property can be successfully improved by optimizing the shape of the panel, as well as the locations and the thicknesses of the stiffeners. About 68% of the total dissipated energy has been increased as a result of optimization from the standard model.

ACKNOWLEDGMENTS

This work is partially supported by the Kajima Foundation's Research Grant, and Grant-in-Aid for Scientific Research (No. 23360248) from JSPS, Japan. Valuable comments by Dr. Yasuda of Taisei Research Institute are also appreciated.

REFERENCES

- Dassault Systems (2011). *ABAQUS Ver. 6.11 Documentation*.
- Glover, F. (1989). "Tabu search: Part I." *ORSA J. Computing*, Vol. 1(3), pp. 190-206.
- Izumi, M., Narihara, H., and Yasuda, S. (1996). "Low cycle fatigue test on shear yielding type low yield stress steel hysteretic damper for response control: Part 6. Test results of width to thickness ratio of web d/t_w -90 series." *Summaries of technical papers of Annual Meeting*, Architectural Institute of Japan, B-2, pp.803-804 (in Japanese).
- Ohsaki, M. (2010). *Optimization of Finite Dimensional Structures*, CRC Press, New York.
- Ohsaki, M., and Nakajima, T. (2012). "Optimization of link member of eccentrically braced frames for maximum energy dissipation." *J. Constructional Steel Research*, Vol. 75, pp. 38-44
- Pan, P., Ohsaki, M., and Tagawa, H. (2007). "Shape optimization of H-beam flange for maximum plastic energy dissipation." *J. Struct. Eng.*, ASCE, 133(8), 1176-1179.
- Watanabe, H., Ohsaki, M., Nozoe, J. and Yasuda, S. (2012). "Shape optimization of shear-type hysteretic steel damper for building frames using FEM-analysis and heuristic approach." *Proc. 7th China-Japan-Korea Joint Symposium on Optimization of Structural and Mechanical Systems (CJK-OSM7)*, Huangshan, China; Paper No. J061.